DRL-58-DRD-SE 7

DOE/JPL 954373 - 78/2
Distribution Category UC-63

HEAT EXCHANGER METHOD — INGOT CASTING
FIXED ABRASIVE METHOD — MULTI-WIRE SLICING
PHASE II

Silicon Sheet Growth Development for the
Large Area Sheet Task of the Low Cost
Silicon Solar Array Project

QUARTERLY PROGRESS REPORT NO. 3

BY

FREDERICK SCHMID AND CHANDRA P. KHATTAK

Covering Period from April 1, 1978 through June 30, 1978

Date of Report: July 15, 1978

JPL Contract No. 954373

CRYSTAL SYSTEMS INC.

Shetland Industrial Park
P.O. Box 1057, Salem, Mass. 01970

The JPL Low-Cost Solar Array Project is sponsored by the U. S. Department of Energy and forms part of the Solar Photovoltaic Conversion Program to initiate a major effort toward the development of low-cost solar arrays. This work was performed for the Jet Propulsion Laboratory, California Institute of Technology by agreement between NASA and DOE.

DRL-58-DRD-SE 7

DOE/JPL 954373 - 78/2
Distribution Category UC-63

HEAT EXCHANGER METHOD - INGOT CASTING
FIXED ABRASIVE METHOD - MULTI-WIRE SLICING
(PHASE II)

Silicon Sheet Growth Development for the Large Area Sheet Task of the Low Cost Silicon Solar Array Project

Quarterly Progress Report No. 3

by

Frederick Schmid and Chandra P. Khattak

Covering Period from April 1, 1978 through June 30, 1978

Date of Report: July 15, 1978

JPL Contract No. 954373

CRYSTAL SYSTEMS, INC.
35 Congress Street
Salem, MA 01970

This work was performed for the Jet Propulsion Laboratory, California Institute of Technology, under NASA Contract NAS7-100 for the U.S. Department of Energy.

The JPL Low-Cost Solar Array Project is funded by DOE and forms part of the Solar Photovoltaic Conversion Program to initiate a major effort toward the development of low-cost solar arrays.

This report contains information prepared by Crystal Systems, Inc., under JPL subcontract. Its content is not necessarily endorsed by the Jet Propulsion Laboratory, California Institute of Technology, National Aeronautics and Space Administration or the U. S. Department of Energy.

TABLE OF CONTENTS

ABSTRACT

Semiconductor grade silica crucibles have been fabricated and used to produce crack-free ingots with almost total single crystallinity. Solar cells fabricated out of HEM cast material have shown conversion efficiencies of 14%. The high V_{oc} and CFF values suggests that this material is purified by the directional solidification.

A very high degree of crystallinity has been achieved in the square ingots cast. High purity square crucibles are being fabricated.

Efficient slicing was carried out with 30 μm and 22 μm diamonds in addition to the 45 μm size. The use of synthetic diamonds gave a poorer performance as compared to the natural kind. The surface damage with 22 μm diamonds was 4-6 μm. The nickel plating after impregnation holds the diamonds if it is suitably hardened by heat treatment.

The projected add-on cost for 1982 and 1986 is $(20.27 - 34.89) and $10.62 per square meter of silicon wafer respectively using the HEM and FAM approaches.

CRYSTAL CASTING

Efforts during this quarter were concentrated in three areas, viz., (i) casting in high purity graded crucibles; (ii) casting square ingots; and (iii) solar cell performance and evaluation.

Casting in High Purity Graded Crucibles

In run 2-041-C (details in Table I) a high-purity crucible was used. This crucible was fabricated as per semiconductor standard and a graded structure was developed to eliminate cracking. The crucible delaminated after cool-down and there was no sign of any cracking of the ingot. Figures 1 and 2 show the cast ingot in the crucible as removed from the furnace and the as-cast surface of the ingot respectively. Figures 3 and 4 show the top and bottom surfaces of the ingot. A portion of the unmelted seed is evident in Figure 4. Since the crucible is mainly supported on the heat exchanger, an impression of the heat exchanger is formed on the bottom of the ingot. In other areas the crucible sags under the weight of the silicon.

In run-2-042-C the procedure of 2-041-C was repeated and again an ingot was cast with no signs of cracking. This ingot was sectioned in order to see the crystallinity. A polished and etched section is shown in Figure 5. It can be seen that

TABLE I. TABULATION OF HEAT-EXCHANGER AND FURNACE TEMPERATURES

RUN	PURPOSE	SEEDING		GROWTH CYCLE			REMARKS
				RATE OF DECREASE			
		FURN.TEMP. ABOVE M.P.	H.E.TEMP. BELOW M.P.	H.E. TEMP. °C/HR.	FURN. TEMP. °C	GROWTH TIME IN HOURS	
2-031-C	Improve delamination of square crucible by heat treatment after growth	22	45	284	22	5.3	Very limited attachment of crucible to ingot
2-032-C (2)	Sample for carbon analysis without use of graphite retainer	5	61	229	5	9.0	Clean top surface, no SiC
2-033-C	Same as 2-031-C	3	83	500	3	5.0	Limited attachment of crucible to ingot
2-034-C	Same as 2-031-C	3	86	327	3	7.5	Limited attachment of crucible to ingot
2-035-C	Same as 2-031-C	23	78	322	23	6.3	Very limited attachment of crucible to ingot
2-036-C	Improve delamination of clear crucible by heat treatment after growth	7	88	292	7	5.2	Attachment of crucible to ingot caused cracking
2-037-C	Casting of square ingot in different type of silica (#29) crucible	19	70	305	19	12.25	Crucible deformed. Cracking limited to corners.

TABLE I. TABULATION OF HEAT-EXCHANGER AND FURNACE TEMPERATURES (cont.)

RUN	PURPOSE	SEEDING		GROWTH CYCLE			REMARKS
				RATE OF DECREASE			
		FURN.TEMP. ABOVE M.P.	H.E.TEMP. BELOW M.P.	H.E. TEMP. °C/HR.	FURN. TEMP. °C	GROWTH TIME IN HOURS	
2-038-C	Casting of square ingot in different type of silica (#30) crucible	18	75	1040	18	5.25	Crucible deformed. Limited cracking.
2-039-C (3)	Cast square ingot in heat treated opaque type II crucible	-	-	-	-	-	Run terminated as crucible failed during heat-up.
2-040-C	Cast square ingot in opaque type II crucible	5	80	343	5	6.0	Limited cracking of ingot.
2-041-C	Cast ingot in high purity graded crucible	4	106	218	4	5.25	No sign of cracking of ingot. Very good crucible delamination.
2-042-C	Same as 2-041-C	5	134	201	5	6.5	Very good crystallinity in the crack-free ingot cast.
2-043-C	Test duplex square crucible	12	120	340	12	5.5	Limited cracking of ingot.
2-044-C	Same as 2-039-C	-	-	-	-	-	Run terminated as crucible failed during heat-up.
2-045-C	Test duplex square crucible with graphite plug	-	-	-	-	-	Run terminated as crucible failed during melt-down.

TABLE I. TABULATION OF HEAT-EXCHANGER AND FURNACE TEMPERATURES (cont.)

RUN	PURPOSE	SEEDING		GROWTH CYCLE			REMARKS
				RATE OF DECREASE			
		FURN. TEMP. ABOVE M.P.	H.E. TEMP. BELOW M.P.	H.E. TEMP. °C/HR.	FURN. TEMP. °C	GROWTH TIME IN HOURS	
2-046-C	Test duplex square crucible	27	93	444	27	6.0	Limited cracking of ingot
2-047-C	Heat treatment of crucible	-	-	-	-	-	Heat treatment satisfactory.
2-048-C (F)	Improve growth rate with high purity crucible	4	96	305	4	5.0	Very good crystallinity achieved.
2-049-C	Improve growth rate with high purity crucible	31	91	296	31	4.0	Good crystallinity. Some cracking of ingot because of improper graded structure of crucible.
2-050-C	Test graded clear crucible	3	133	242	3	6.0	Ingot cracked due to attachment to crucible
2-051-C	Improve growth rate with graphite plug	-	-	-	-	-	Run aborted. Crucible cracked around plug.

Figure 1. Ingot cast (#2-041-C) in high purity graded silica crucible.

Figure 2. As-cast surface of 6" diameter ingot (#2-041-C)

Figure 3. Top surface of ingot cast in run 2-041-C

Figure 4. Bottom surface of ingot cast in run 2-041-C

except for the areas near the edges the silicon is mono-crystal. The areas of twinning are the portions of the bottom where the crucible has sagged under the weight of silicon and, therefore, growth has initiated from the bottom of the crucible instead of from the seed. In order to study the uniformity of the structure this ingot was sectioned into four pieces by slicing vertically twice and then sectioning one of the pieces horizontally. The polished and etched sliced surfaces of these sections are shown in Figure 6. It can be seen that the uniformity of structure of the ingot is very good and Figure 5 shows a good representation of crystallinity.

The growth rate was increased from 0.5 to 0.6 kg/hr for run 2-048-C. It was found that these higher growth rates did not affect the crystallinity of the cast ingot, as evident from the polished and etched section in Figure 7.

Casting Square Ingots

In order to cast square cross-section ingots by HEM, square crucibles are required. These crucibles are not available off the shelf and have to be custom-made. These crucibles do not have the desired graded structure to prevent cracking of the ingot. Some vendors have encountered problems in making the desired shape and have thus not delivered the crucibles.

Figure 5. Polished and etched section of 2-042-C

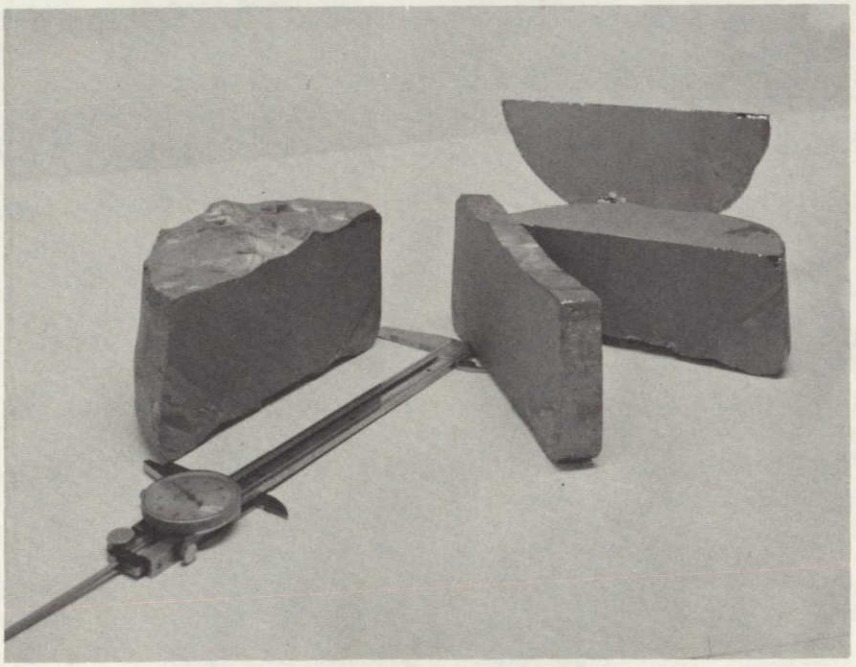

Figure 6. Polished and etched sections of 2-042-C

Figure 7. Polished and etched section of 2-048-C.

During last quarter[1] it was felt that since the square crucibles received in-house are potentially cheap, it may be worth adapting them to cast crack-free ingots. During this quarter delamination of the crucible was attempted by heat treatment after the ingot has been solidified. This was done with a view to break down the silicon/silica bond and thereby decrease attachment of the crucible to the ingot and prevent cracking. Runs #2-031-C and 2-033-C through 2-035-C (Table I) were carried out under these experimental conditions. The attachment of the crucible was considerably reduced as is evident from a view of the ingot cast in run #2-031-C (Figure 8). It can be seen that the attachment and thereby cracking was limited to one corner. As far as crystal growth, solidification was complete into the corners. The cavity seen in Figure 8 was developed because of a leak in the crucible in that area. The bottom of the ingot did not show any attachment to the crucible.

The heat treatment after solidification was successful in limiting the cracking. It was felt that the same treatment be tried for clear silica crucibles; hence, run 2-036-C was attempted. The cracking could not be limited in this experiment.

Aside from using heat-treatments to enhance delamination three different types of silica were used to fabricate square crucibles. These have different sintering characteristics and hence are expected to show a different delamination behavior. Runs 2-037-C and 2-038-C were carried out using this approach.

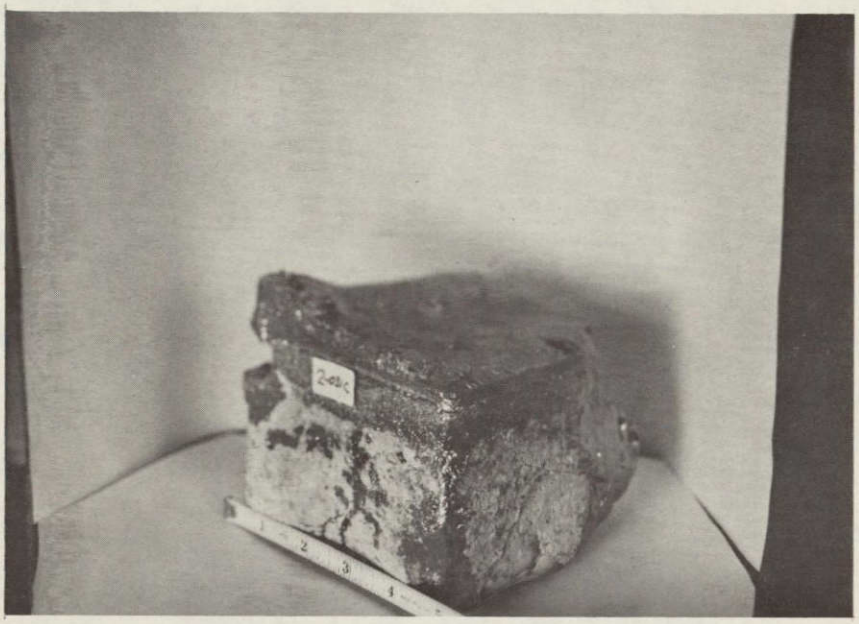

Figure 8. A view of the square ingot cast in run 2-031-C

It was found that in both cases the phase transformations and sintering in these crucibles caused deformation of the crucible so that the cast shape was no longer a square cross-section.

The crystallinity of the cast material has been very good. This is illustrated from the polished and etched cross-sections of two square ingots cast in run 2-034-C and 2-035-C in Figure 9. On crucibles for runs 2-039-C and 2-044-C heat treatment was carried out to develop a graded structure. In these experiments it was found that the thermal cycling because of heat treatment and heat-up cycle cracked the crucible and the run had to be aborted. No delamination of the crucible took place but the cracking of the crucible during melt-down forced termination of the run.

The square crucibles used so far have not been fabricated under high purity specifications. One way to achieve high purity is to use a high purity liner inside these crucibles. Such duplex crucibles have been fabricated and tested in runs 2-043-C and 2-046-C. Figure 10 shows top views of square ingots cast in a duplex crucible. Some minor cracking of the ingots can be seen. Figure 11 shows a side view of one ingot. It can be seen that there was no problem of silicon solidifying in the corners of the crucible. The attachment of the crucible to the cast ingot occurred only in certain areas; hence, the ingot cracking was rather limited.

Fabrication of square cross-section crucibles of high purity similar in structure to those used in runs 2-041-C and 2-042-C is in progress.

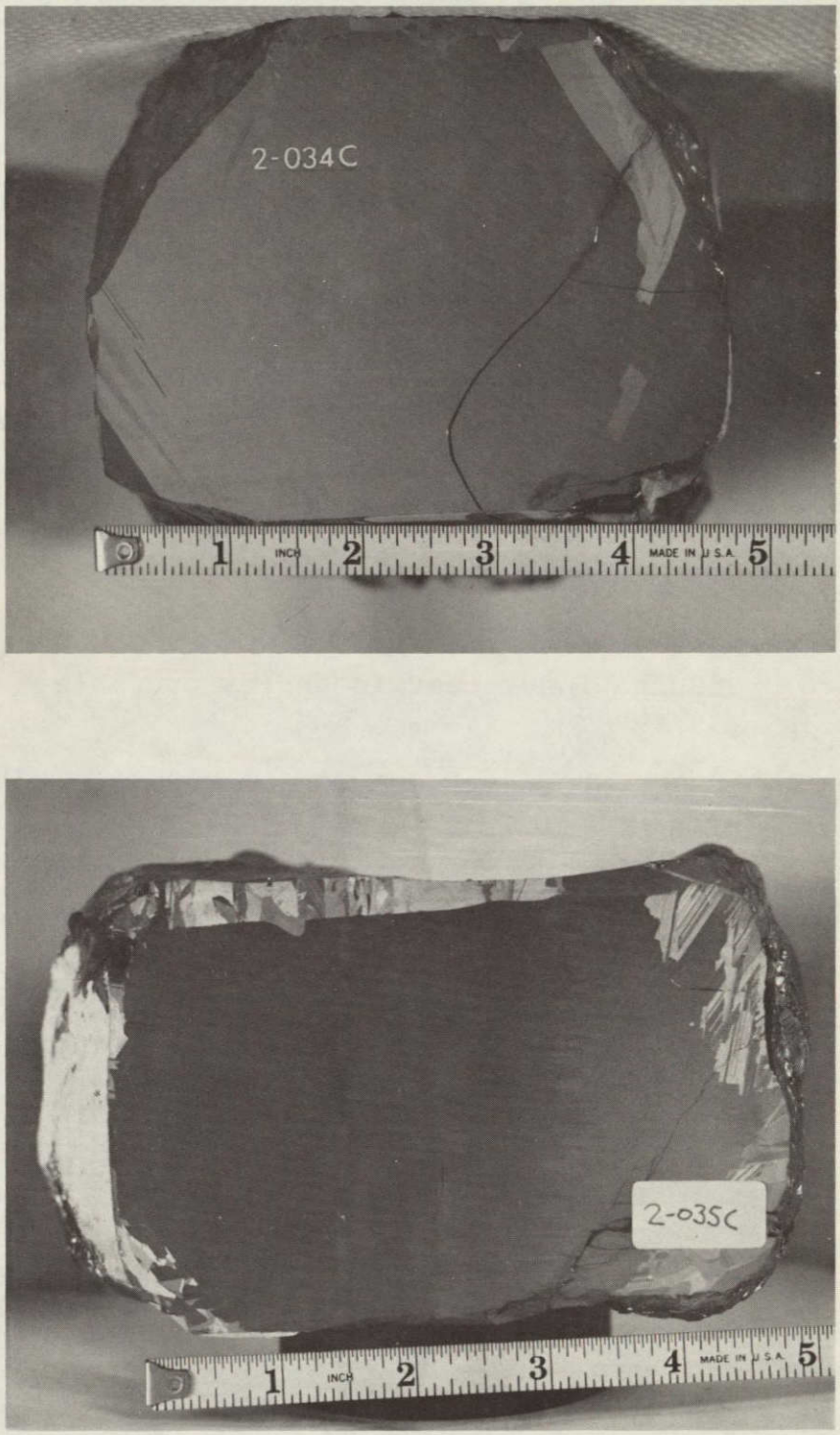

Figure 9. Polished and etched cross-sections of square ingots cast in run 2-034-C (above) and 2-035-C (below)

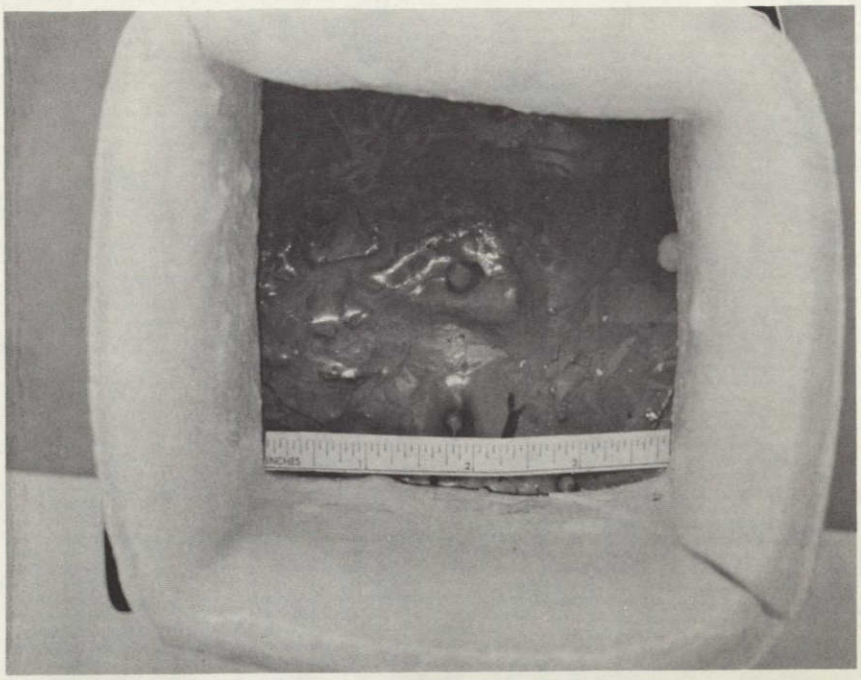

Figure 10. Square ingot cast in duplex crucible (#2-043-C)

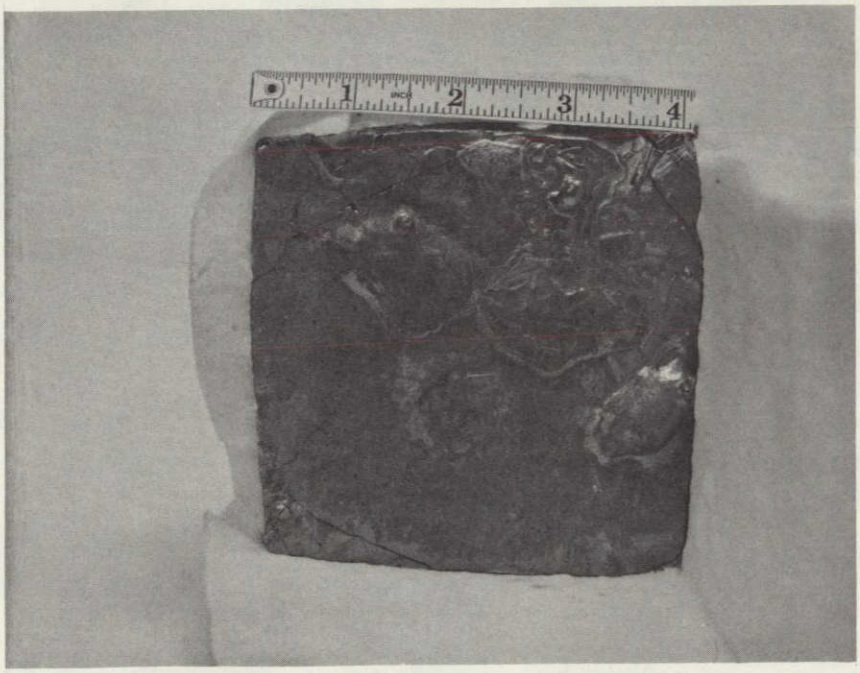

Figure 11. As-cast surface of square ingot (#2-046-C)

SiC Impurities

It has been established[2] by thermodynamic analysis that SiC is formed at high temperatures in vacuum melting of silicon. The reaction responsible for SiC formation is

$$2Si + CO \rightarrow SiC + SiO$$

The source of CO, aside from a vacuum leak, is from reactions between silica crucible and graphite retainer, viz.

$$3C + SiO_2 \rightarrow SiC + 2CO$$

$$C + SiO_2 \rightarrow SiO + CO$$

These reactions become operative when the pressure drops below 10 torr near the melting point of silicon.

This theoretical data has been experimentally verified by not using graphite retainers. In these runs it was found the melt was cleaner, surface of cast ingot was shiny and the crystallinity was improved. Some of the samples were analyzed for carbon by infrared analysis and the data is shown in Table II. It was found that when a graphite retainer was used the carbon levels were close to the solubility limit of carbon in silicon. However, when a graphite retainer was not used, the carbon levels were reduced by approximately 50%. The variation in carbon level is associated with the vacuum conditions in the furnace. It may be important to point out that whenever the graphite retainer was used, the carbon level was more than 3×10^{17} atoms/cc. The low values of $(1.5 - 3) \times 10^{17}$ atoms/cc carbon have only been achieved when graphite retainer has not been used in the HEM growth of silicon.

TABLE II. CORRELATION OF CARBON CONTENT IN MELT WITH USE OF GRAPHITE RETAINER

Run #	Graphite Retainer Used	Carbon atoms/cc x 10^{17}
70-C	Yes	3.71
109-C	Yes	3.59
109-C	Yes	3.46
115-C	Yes	4.07
115-C	Yes	4.08
2-021-C	No	2.59
2-021-C	No	2.24
2-032-C	No	1.97
2-032-C	No	1.54
2-032-C	No	2.21
2-032-C	No	3.02
2-032-C	No	2.16
2-032-C	No	3.14

It has been found that even when the carbon levels have been close to solubility limit, SiC floats on the surface, but the crystallinity by HEM has been high, unlike the Czochralski process.

Solar Cell Performance

In the HEM casting different types of crucibles have been used to obtain a crack-free ingot. Some of these crucibles have been fabricated from low-cost silica that does not

meet semiconductor purity standards. This resulted in contamination of the ingot and possibly the furnace. It has been established[2] that when vacuum melting the use of graphite retainers in contact with SiO_2 results in formation of silicon carbide and high carbon levels in the melt. It was, therefore, intended to study the effect of the solar cell performance as a function of (i) purity of the crucible; (ii) crystallinity; and (iii) carbon level. Six ingots cast by the HEM were processed into solar cells for this study.

Ingot samples were checked for resistivity, sliced into six nominal 0.46 mm (18 mils) wafers, chemically polished and checked for resistivity again. The details of the samples are shown in Table III.

The standard cell processing technique utilized a phosphine gas diffusion at a temperature of 850°C to yield a sheet resistance of about 45 ohms/square (V/I ∿ 10) on Czochralski-grown, aerospace type 1-3 ohm-cm control material. This gives a diffusion depth of approximately 0.4 microns which is adequate under normal processing to prevent evaporated contact metal from shunting across the N/P junction. The gridline spacing, 9 gridlines/cm for 2 x 2 cm cells and 10 gridlines/cm for the 1 x 2 cells was designed to minimize series resistance due to sheet resistance of the diffused layer. The "N" and "P" contacts were vacuum evaporated silver-titanium and AR coating was Ta_2O_5. All cells were further processed to remove any metallization that may have been deposited across the N/P junction along the cell perimeter.

TABLE III. DETAILS OF CASTING OF SIX INGOTS FABRICATED INTO SOLAR CELLS

Run Number	Crucible	Doped	Crystallinity	Graphite Retainer Used	Resistivity (ohm-cm)
2-021-C	High purity	Yes	Good	No	4.3 - 4.6
95-C	High purity	Yes	Good	Yes	5.3 - 5.8
70-C	High purity	Yes	Twinned	Yes	10.9 - 14.6
2-028-C	High purity graded	No	Good	No	46 - 64
119-C1	Low purity	Yes	Good	No	5.1 - 9.7
119-C2	Low purity	Yes	Twinned	No	5.1 - 6.4

As can be seen from the above details, the cell processing was not optimum for each ingot sample but, rather, tailored to avoid shunting effects due to grain boundaries present in some samples. Further, all the samples were processed as one batch so that the possibility exists that the impurities from one sample could contaminate the other samples during the diffusion process. Three control samples were run along with the test samples. They were placed in the front (F), center (C), and back (B) with respect to gas flow during diffusion.

All cells were tested under a Xenon light source at AMO intensity of 135.3 mW/cm^2 using a standard cell. The test block temperature was 24°C. The data is tabulated in Table IV.

As small as the difference may be, it is interesting to note that of the control cells, the one in front (F cell) with respect to the gas flow showed the highest efficiency. Further, one of the cells from ingot 2-021-C showed a conversion efficiency which was higher than all the control cells. A comparison of the data of the control cells and cells from run 2-021-C shows that the test cells show consistently high V_{oc} and low I_{sc} values. Since the material is expected to be contaminated by impurities from the furnace, low values of I_{sc} are expected. The high values of V_{oc} are rather high for a material with 4.3-4.6 ohm-cm resistivity. The V_{oc} expected from Czochralski-grown material in this resistivity range is about 570 mV. The V_{oc} value of 525 mV for cell 5 from run 2-028-C is also high for material of 46-64 ohm-cm resistivity.

TABLE IV. SOLAR CELLS TESTED UNDER AMO CONDITIONS (135.3 mW/cm^2)

Ingot	#	Area (cm^2)	I_{sc} (mA)	V_{oc} (mV)	I_{mp} (mA)	V_{mp} (mV)	P_{max} (mW)	FF	η
Control	F	4.02	137.2	589	131.0	490	64.2	0.794	11.8
	C	4.02	136.0	590	129.0	495	63.8	0.796	11.7
	B	4.02	136.2	591	127.8	500	63.9	0.794	11.7
2-021-C	1	4.02	130.2	615	121.4	515	62.5	0.781	11.5
	2	4.02	131.8	614	122.8	520	63.8	0.789	11.7
	3	4.02	129.2	613	121.2	520	63.0	0.796	11.6
	4	4.02	132.2	617	122.8	525	64.5	0.790	11.9
	5	4.02	130.8	615	124.0	520	64.5	0.802	11.9
	6	4.02	128.5	615	121.8	525	63.9	0.810	11.7
95-C	1	4.02	98.6	576	91.6	480	44.0	0.774	8.1
	2	4.02	90.4	569	83.4	475	39.6	0.770	7.3
	3	4.02	100.5	574	91.8	475	43.6	0.756	8.0
	4	4.02	90.6	564	85.2	470	40.0	0.784	7.4
	5	4.02	98.1	567	81.0	455	36.9	0.663	6.8
	6	4.02	101.6	568	83.0	460	38.2	0.662	7.0
70-C	1	2.01	41.2	524	34.5	420	14.5	0.671	5.3
	5	2.01	39.0	504	31.4	390	12.2	0.623	4.5

TABLE IV. SOLAR CELLS TESTED UNDER AMO CONDITIONS (135.3 mW/cm^2) (cont.)

Ingot	#	Area (cm^2)	I_{sc} (mA)	V_{oc} (mV)	I_{mp} (mA)	V_{mp} (mV)	P_{max} (mW)	FF	η
2-028-C	4	2.01	60.7	486	47.4	340	16.1	0.546	5.9
	5	2.01	60.2	552	51.3	450	23.1	0.695	8.5
119-C1	1	4.02	77.6	522	63.5	405	25.7	0.635	4.7
	2	4.02	78.9	538	70.6	440	31.1	0.732	5.7
	3	4.02	100.5	551	91.8	455	41.8	0.754	7.7
	4	4.02	83.4	544	77.1	455	35.1	0.773	6.5
	5	4.02	91.8	554	80.8	455	36.8	0.749	6.8
	6	4.02	85.8	542	77.4	450	34.8	0.728	6.4
119-C2	1	4.02	83.0	534	69.4	420	29.2	0.685	5.4
	2	4.02	81.8	508	66.0	370	24.4	0.588	4.5
	3	4.02	79.3	507	63.1	375	23.7	0.589	4.4
	4	4.02	77.8	476	61.5	340	20.9	0.565	3.8
	5	4.02	70.7	443	56.8	300	17.0	0.544	3.1
	6	4.02	81.8	531	69.4	420	29.1	0.671	5.4

In the Heat Exchanger Method the motionless directional solidification may distribute impurities and dopant similar to the float zone technique. Therefore, the material cast by the HEM may be similar to float-zone silicon where higher V_{oc} and FF values are also observed. Further, the junction formed in these cells is about 0.4 microns. If a shallower junction is formed, which is optimum for this material, better performance could be achieved from these cells.

In an effort to study the performance of the cells from run 2-021-C under terrestrial conditions, the I-V characteristics were measured under AM1 conditions. Data was taken under Xenon as well as tungsten illumination and the results are shown in Table V. It can be seen that conversion efficiencies as high as 14% have been achieved in spite of the impurities expected in the material. A comparison of the data under Xenon and tungsten light source shows that there is more of the blue response than the red response. The Ta_2O_5 AR coating is expected to help the blue response.

A comparison of this data with run 95-C shows that there is decrease in solar cell performance in cells from 95-C. In this run a graphite retainer was used in contact with silica crucible, thus the carbon levels in silicon are expected to be high. Even though the effect of carbon levels in silicon may not be as drastic as the values indicate, it does show that high carbon levels degrade the solar cell performance.

TABLE V. I-V Parameters under AM1 conditions for AR coated (Ta_2O_5) solar cells fabricated from run 2-021-C using Xenon and Tungsten source illumination.

Sample #	Xenon Source				
	I_{sc} (mA)	V_{oc} (mV)	CFF	P_{max} (mW)	η (%)
1	114.2	609	0.771	53.6	13.3
2	116.8	612	0.764	54.6	13.6
3	114.5	610	0.784	54.8	13.6
4	117.2	615	0.782	56.4	14.0
5	116.2	613	0.784	55.9	13.9
6	113.3	612	0.792	54.9	13.7
Mean	115.4	612	0.780	55.0	13.7

Sample #	Tungsten Source				
	I_{sc} (mA)	V_{oc} (mV)	CFF	P_{max} (mW)	η (%)
1	95.9	598	0.771	44.2	11.0
2	99.0	602	0.770	45.9	11.4
3	95.5	599	0.787	45.0	11.2
4	100.2	605	0.784	47.6	11.8
5	98.0	602	0.789	46.6	11.6
6	97.0	602	0.788	46.0	11.4
Mean	97.6	601	0.782	45.9	11.4

The decrease in efficiency with poor crystallinity is shown by the cell characteristics from run 70-C which had a twinned structure as compared to 95-C which had good crystallinity. This is also confirmed by comparing data from run 119-C1 and 119-C2. Both samples were from the same ingot cast in a low-purity crucible, without the use of a graphite retainer. The samples from 119-C1 had better crystallinity and higher efficiency than those from 119-C2. Cell performance of samples from run 119-C show a drastic effect of low purity crucibles when compared to the values from run 95-C and 70-C.

Solar cell #2-021-C-4 was measured for spectral response and the data is shown in Table VI. A review of this data shows that the peak is between 0.8 and 0.9 μm wavelength, similar to conventional cells; however, the response at low wavelengths is higher. This low-wavelength response could be further improved if a shallower junction had been made on the cell.

In conclusion, it has been found that conversion efficiencies of up to 14% have been achieved in solar cells fabricated out of HEM cast silicon in a contaminated furnace. The silicon acts more like a float zone than Czochralski material. The purity of the crucible, crystallinity of the cast ingot, and carbon levels in silicon all have detrimental effect on the solar cell performance.

TABLE VI. Spectral Response, R, of Test Solar Cell # 4

λ μm	R mA/mW	R/R_{max} %
0.4	0.1405	27.3
0.45	0.2616	50.8
0.5	0.3547	68.9
0.6	0.4319	83.9
0.7	0.4809	93.5
0.8	0.5145	100.0
0.9	0.4846	94.2
0.95	0.4255	82.7
1.00	0.2353	45.7

CRYSTAL SLICING

Efforts in crystal slicing were directed towards blade development, testing and characterization of wire blades and wafer surfaces.

Slicing Tests

Slicing tests were carried out with a view to develop an optimum blade with respect to (i) plated or impregnated; (ii) diamond size; (iii) sulfamate or electroless coating after impregnation; (iv) hardness of the coating; (v) thickness of coating. The first four variables have been addressed during this period.

During the last quarter[1] some testing was carried out with blades heat treated after electroless nickel plating. This was continued with run 2-020-S (Table VII) when the heat treatment was at 600°F. It was found that because of this heat treatment the nickel was very hard and embrittled resulting in delamination; hence, the run was aborted. Since the 500°F heat treatment in run 2-018-S[1] seems to adhere the coating onto the wire, runs 2-021-S and 2-022-S were carried out with similar parameters and blade, but using 30 μm diamonds to compare with the 45 μm size used earlier. In run 2-021-S explosively formed synthetic

TABLE VII. SILICON SLICING SUMMARY

RUN	PURPOSE	FEED FORCE/BLADE lb	FEED FORCE/BLADE gm	AVERAGE CUTTING RATE mil/min	AVERAGE CUTTING RATE mm/min	WIRE TYPE	REMARKS
2-020-S	Life test commercially impregnated wire with high temperature heat treatment (600°F)	N/A	N/A	N/A	N/A	Commercial 8 mil, 0.2 mm impregnated 45 μm diamond; 0.5 mil, 12.5 μm electroless nickel plated	Run aborted. Embrittlement of coating due to heat treatment
2-021-S	Life test CSI impregnated with synthetic diamonds wire	0.083	37.7	1.42	0.036	5 mil, 0.125 mm tungsten core, 0.7 mil, 17.5 μm copper sheath, 30 μm synthetic diamonds CSI impregnated; 0.3 mil, 7.5 μm electroless nickel plated, 500°F heat-treated	Good wafer quality. Cutting rates low towards the end of the run.
2-022-S	Life test CSI impregnated with natural diamonds wire	0.083	37.7	2.62	0.067	Similar to 2-021-S but with 30 μm natural diamonds	Good wafer quality. Very good cutting rates.
2-023-S	Life test	0.083	37.7	1.45	0.037	Same as 2-022-S	Good wafer quality.
2-024-S	Life test	0.085	38.6	2.32	0.059	Similar to 2-020-S but with sulfamate nickel coating.	Good wafer quality. Excessive nickel build-up.
2-025-S	Life test	0.085	38.6	2.02	0.051	Same as 2-024-S.	Good wafer quality.
2-026-S	Life test	0.085	38.6	1.62	0.041	Same as 2-024-S.	Good wafer quality.

TABLE VII. SILICON SLICING SUMMARY (Cont.)

RUN	PURPOSE	FEED FORCE/BLADE lb	FEED FORCE/BLADE gm	AVERAGE CUTTING RATE mil/min	AVERAGE CUTTING RATE mm/min	WIRE TYPE	REMARKS
2-027-S	Life test CSI impregnated wire	0.097	44.0	1.87	0.047	5 mil, 0.125 mm tungsten core, 0.3 mil, 7.5 μm copper sheath, 45 μm diamonds CSI impregnated; 0.5 mil, 12.5 μm sulfamate nickel coating	Nickel coating needed dressing; fair quality wafers due to wire wander
2-028-S	Life test	0.083	37.7	1.71	0.043	Same as 2-027-S	Fair wafer quality due to wire wander
2-029-S	Life test	0.083	37.7	1.36	0.035	Same as 2-027-S	Fair wafer quality due to wire wander
2-030-S	Life test	0.152	69.0	2.5	0.064	Same as 2-027-S	Fair wafer quality due to wire wander
2-031-S	Life test	0.138	62.7	2.3	0.058	Same as 2-027-S	Fair wafer quality due to wire wander
2-032-S	Test effect of heat treatment, compared to runs 77-S thru 79-S	0.080	36.3	1.41	0.036	Commercial 8 mil, 0.2 mm impregnated 45 μm diamond; 0.3 mil, 7.5 μm electroless nickel plated	The cutting performance was poorer for the unheat-treated blades.
2-033-S	Life test	0.080	36.3	0.63	0.016	Same as 2-032-S	The blades suffered from diamond pull-out.

TABLE VII. SILICON SLICING SUMMARY (cont.)

RUN	PURPOSE	FEED FORCE/BLADE lb.	FEED FORCE/BLADE gm	AVERAGE CUTTING RATE mil/min	AVERAGE CUTTING RATE mm/min	WIRE TYPE	REMARKS
2-034-S	Test sulfamate nickel coating	0.080	36.3	2.05	0.052	Commercial 8 mil, 0.2 mm impregnated 45 μm diamond; 0.3 mil, 7.5 μm sulfamate nickel plated	Good wafer quality
2-035-S	Life test	0.080	36.3	1.25	0.032	Same as 2-034-S	Good wafer quality. Diamond pull-out apparent.
2-036-S	Test effect of heat treatment, compared to runs 2-032-5 and 2-033-S	0.080	36.3	1.58	0.040	Commercial 8 mil, 0.2 mm impregnated 45 μm diamond; 0.3 mil, 7.5 μm electroless nickel plated	Diamond pull-out possible.
2-037-S	Life test	0.080	36.3	1.16	0.029	Same as 2-036-S	Run aborted due to poor cutting rates.

diamonds were impregnated while in run 2-022-S natural diamonds were used. Since smaller diamonds were used the nickel plating after impregnation was reduced from 0.5 mil, 12.5 μm to 0.3 mil, 7.5 μm. A comparison of the data obtained shows that 30 μm diamonds will cut efficiently; however, the performance of the synthetic diamonds is poorer than the natural under similar conditions.

In order to compare the effect of the nickel coating after impregnation, a blade pack plated with sulfamate nickel was used in run 2-024-S. The nickel plating obtained was thicker on the outer wires. This resulted in bridging of the outer wires. They were mechanically separated and used in run 2-024-S through 2-026-S to cut through four inches of silicon. Good cutting performance was achieved, i.e., wafer accuracy and yield were good, even though the conditions were not optimum. Examination of the wires with an optical microscope showed minimum diamond pull-out.

In an effort to reduce kerf the thickness of the copper sheath was reduced. A blade pack using a 5 mil, 0.125 mm core and 0.3 mil, 7.5 μm sheath was impregnated with 45 μm diamonds by the Crystal Systems technique. These wires were plated with sulfamate nickel, and again bridging of some wires occurred requiring mechanical separation. This blade pack was used in runs 2-027-S through 2-031-S. The emphasis in these runs was not so much on wafer quality but to determine if diamond pull-out would occur. As has been experienced in the past the higher feed forces gave

higher cutting rates, but wire wander was encountered. The wire wander was attributed to non-uniformity of nickel coating because of bridging and mechanical separation. The data in these runs indicates that diamond pull-out is prevented. It is important to note that 45 μm size diamonds have been impregnated in a copper sheath which is only 7.5 μm thick. On top of this sheath, a nickel coating of 12.5 μm still leaves 25 μm of 45 μm diamonds exposed for cutting. Therefore, this emphasizes the fact that as long as the diamond is exposed and prevented from pull-out, it shows good cutting performance.

Characterization of a blade-pack of 75 wires plated with 0.3 mil, 7.5 μm sulfamate nickel showed that the wires near the edge of the pack had 0.4 to 0.5 mil nickel plating while those near the center had 0.3 mil coating. The nickel coating around each wire was uniform; however, the thickness varied with the position of the wire in the pack. This variation is caused by a non-uniform electric field around the wires. This was minimized by changing the geometry of the wires in the plating bath.

Blade Development

The electroless nickel plating on the blades is hardenable by heat treatment. Sample wires were hardened at different temperatures and their hardness measured. The data is tabulated in Table VIII for electroless and sulfamate (electroplated) nickel. It can be seen that there is a sharp increase in hardness when the blades are heat-treated between 400 and 600°F. At

higher temperatures the hardness is increased sufficiently so that embrittlement takes place. This has been demonstrated in run 2-020-S. A decrease in hardness is observed in sulfamate nickel coating with heat treatment.

TABLE VIII

HARDNESS OF NICKEL COATING AFTER HEAT TREATMENT

Temperature °F	Hardness (Vickers)	
	Electroless Ni	Sulfamate Ni
375	569	405
400	576	378
500	700	382
575	965	368
707	1023	373

To duplicate the blades used in runs 77-C, 78-C, and 79-C, commercially available wires 5 mil core, 1.5 mil copper sheath impregnated with 45 μm diamonds were plated with 0.3 mil electro and electroless nickel.

In both cases, poor cutting performance was experienced with low initial cutting rates and low life. Runs 2-032-S and

2-033-S were a duplication of runs 77-S, 78-S, and 79-S with the exception of not heat treating the blade pack at 375°F. It was not heat treated to retain ductility, for it was felt that the 569 VH may be too hard and brittle. Electro nickel coatings are softer (405 VH) than electroless nickel plated wires. SEM examination of the used and unused wire blades from all runs, as shown in Figure 12, reveals that the diamond concentration on all the unused blades is about the same. SEM examination of the used blades (Figure 13) revealed considerably more diamond pull-out from the blades with softer nickel plating, i.e., unheat-treated. An examination of the longitudinal sections in Figure 12(a) and (b) shows wear marks on the coating which are not evident in Figure 12(c). An examination of the end views of these wires shows that most of the nickel coating is abraded in Figures 13(a) and (b) while it is still present in Figure 13(c). Poor cutting performance was experienced when most of the diamonds pulled out and further cutting wore the coating. However, as long as diamonds stood up, good cutting rates were obtained and there was no wear of the coating.

In runs 2-016-S and 2-017-S the blade pack used was electro-plated with 22 μm diamonds. Kerf losses of 6.2 mil, 0.155 mm were obtained with 100% yield and good quality wafers. These wires were examined with a SEM. Figure 14 shows the unused blade pack with the wire surfaces rotated 180°. Similar examination of the used wires in Figure 15 shows that there is still a high concentration of diamonds left on the cutting edge. This establishes that 22 μm diamonds can be used for slicing.

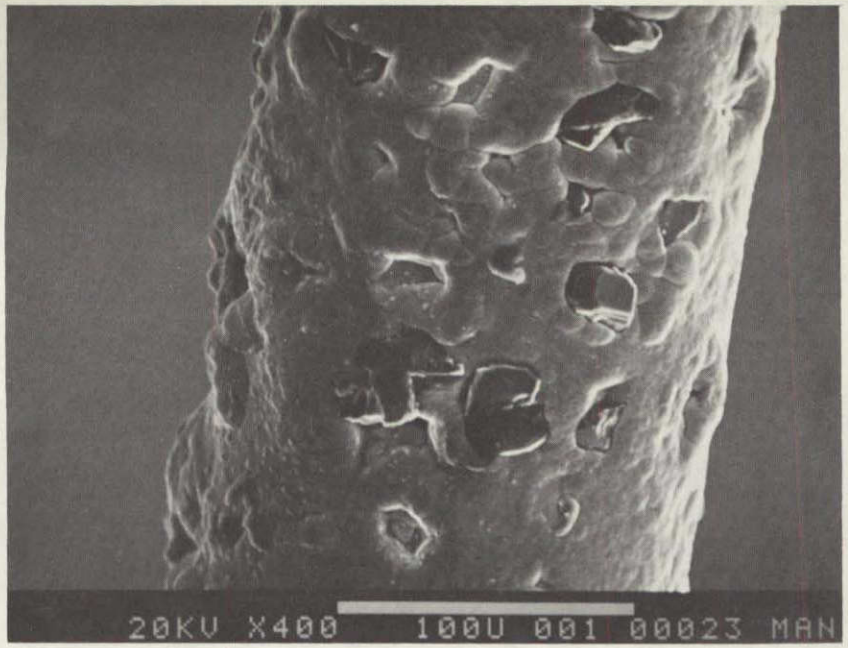

(a) Impregnated wires electroless plated 0.3 mil nickel before use in runs 2-032-S and 2-033-S

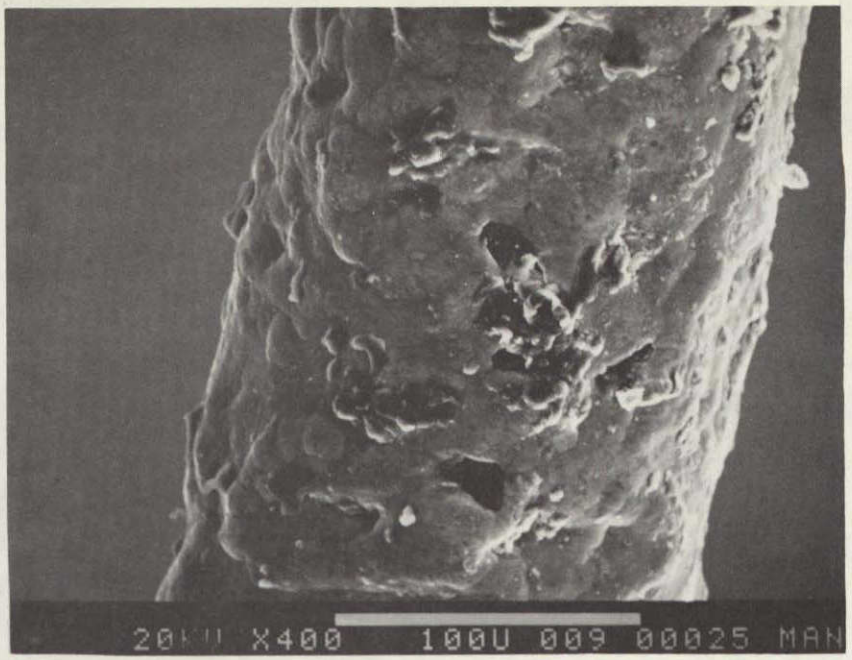

(b) Impregnated wires electroplated with 0.3 mil nickel before use in runs 2-034-S and 2-035-S

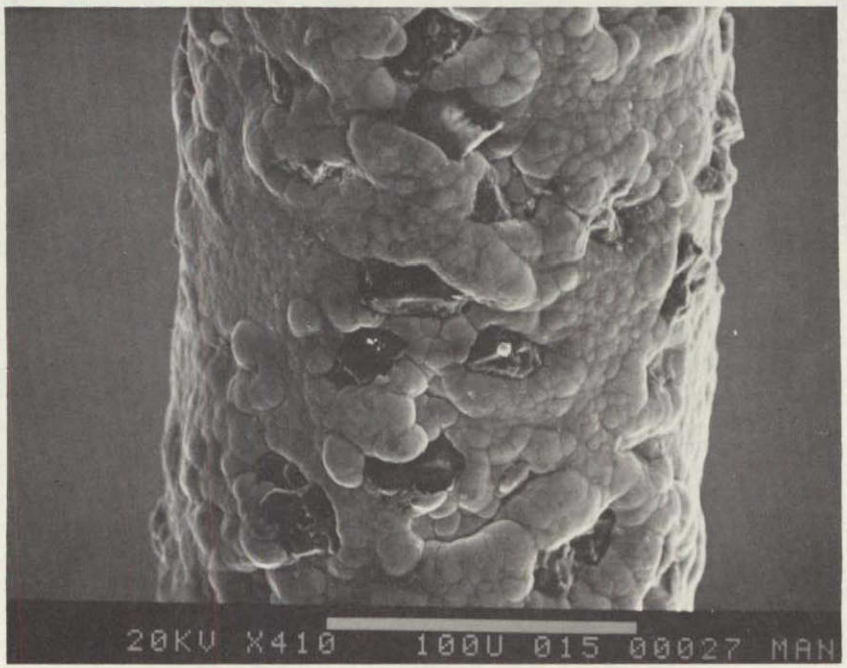

(c) Wires electroless plated 0.3 mil nickel heat treated 375°F before use in runs 77-S through 79-S

Figure 12.

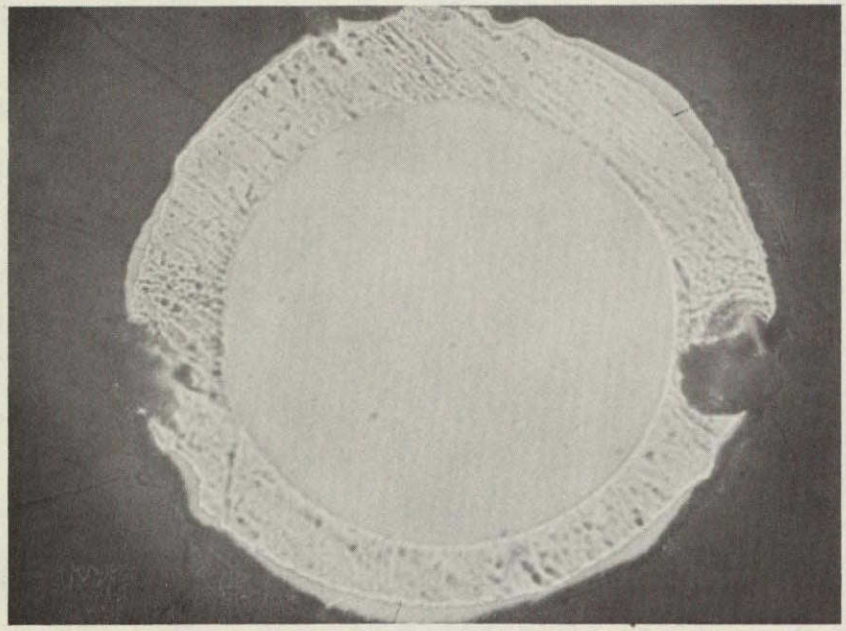

(a) Cross-section of wire electroless plated with 0.3 mil nickel used in runs 2-032-S and 2-033-S

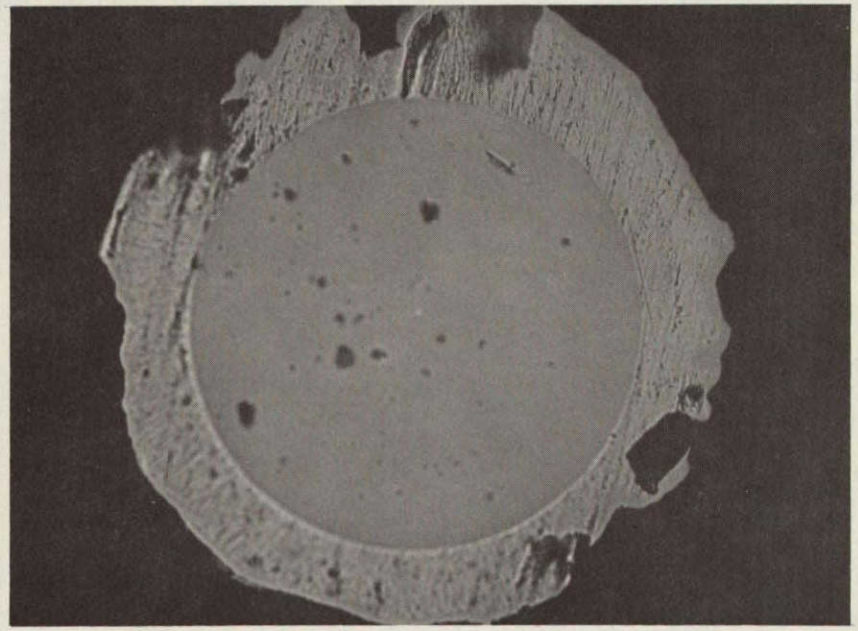

(b) Cross-section of wire electroplated with 0.3 mil nickel used in runs 2-034-S and 2-035-S

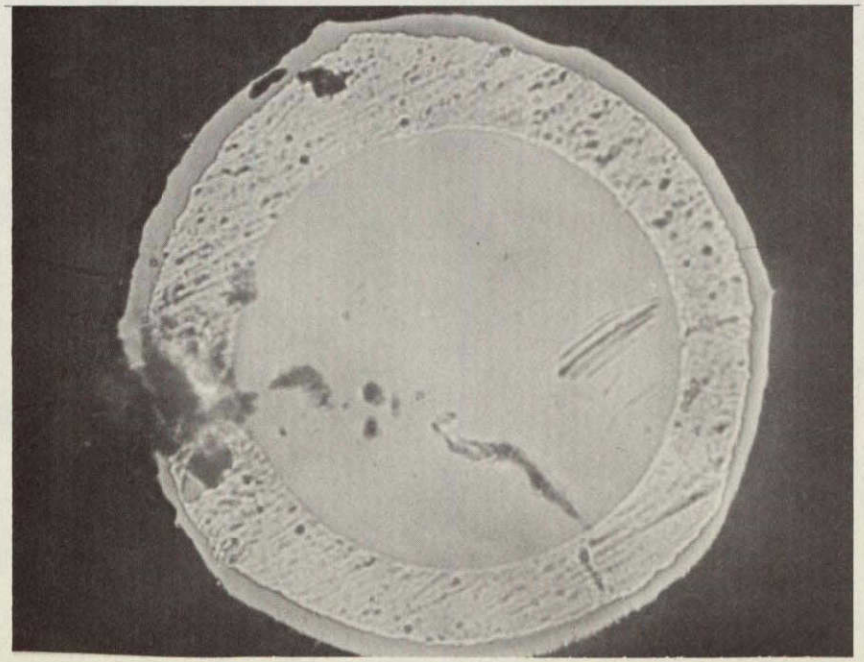

(c) Cross-section of wire electroless plated with 0.3 mil nickel 375°F heat treated used in runs 77-S through 79-S

Figure 13.

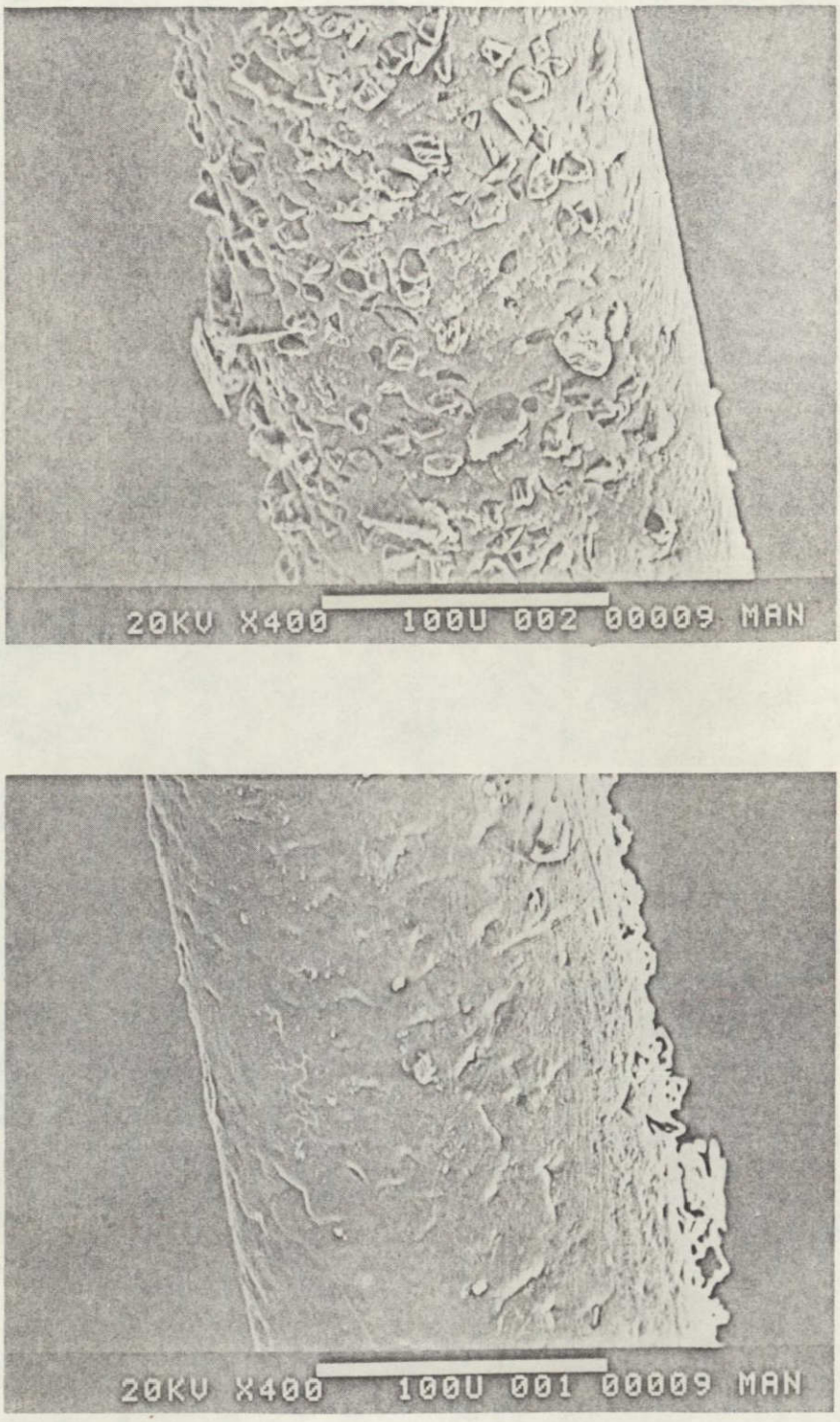

Figure 14. SEM examination of unused blades with 22 μm diamonds. The two sections are rotated 180°.

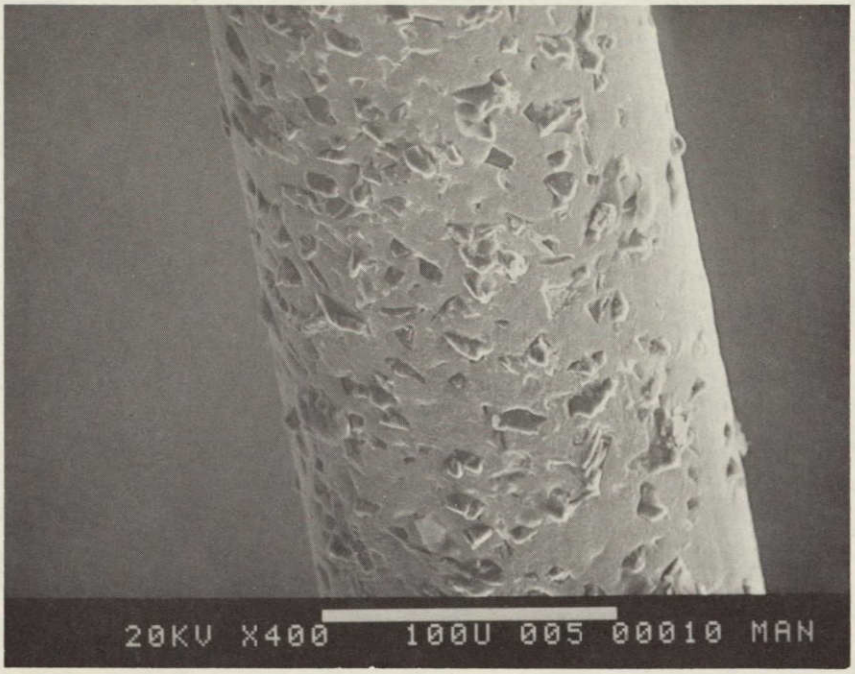

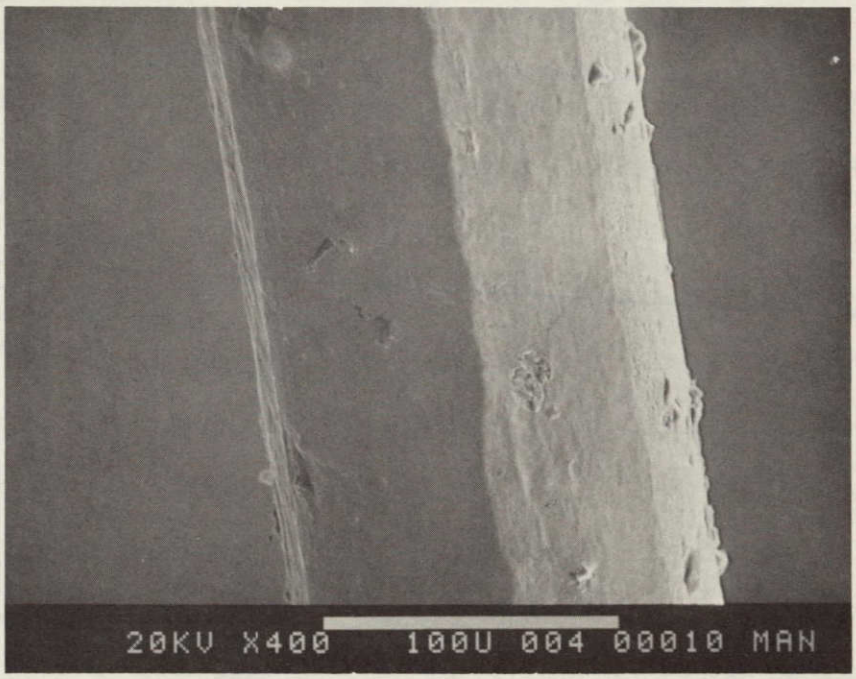

Figure 15. Wire in Figure 14 after use in runs 2-016-S and 2-017-S. The top section is the cutting surface and the bottom section rotated 180°

Characterization of Work Damage

It has been established that the surface damage obtained by fixed abrasive multi-slicing technique is about 5 μm. This has been characterized using 45 μm diamonds. During the last quarter[1] 22 μm diamonds yielded low kerf, 100% yields and very good surface quality. Therefore, these wafers were examined for surface damage. The evaluation was carried out using the technique similar to one adopted earlier[1], viz. preparing a tapered section on the protected sliced surface and examination of a (110) surface perpendicular to the sliced surface. In the earlier work the sliced surfaces were (111); however, in 2-016-S it was (100).

The as-polished and etched tapered sections are shown in Figure 16. The mechanical magnification because of taper is 10X. In the etched section, unlike earlier analysis, the dislocations are not visible in the damaged layer. The extent of surface damage is decided by the extent of microfissures in the sample. The absence of dislocations may be because the surface examined is (100) rather than (111) in the earlier study. Silicon is known to show different etching behavior with orientation. It is felt that this is the explanation rather than the use of 22 μm diamonds as against 45 μm.

The cross-section of the wafer oriented as (110) is shown in Figure 17 in as-polished and etched condition. The extent of surface damage obtained by both the methods shows it to be 4-6 μm which is similar to that found earlier.

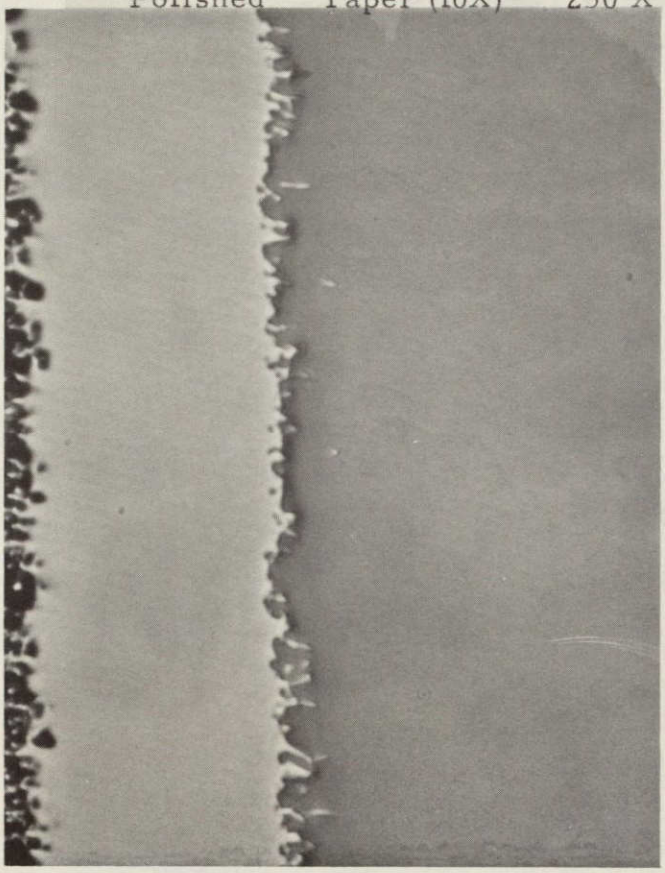

(a)

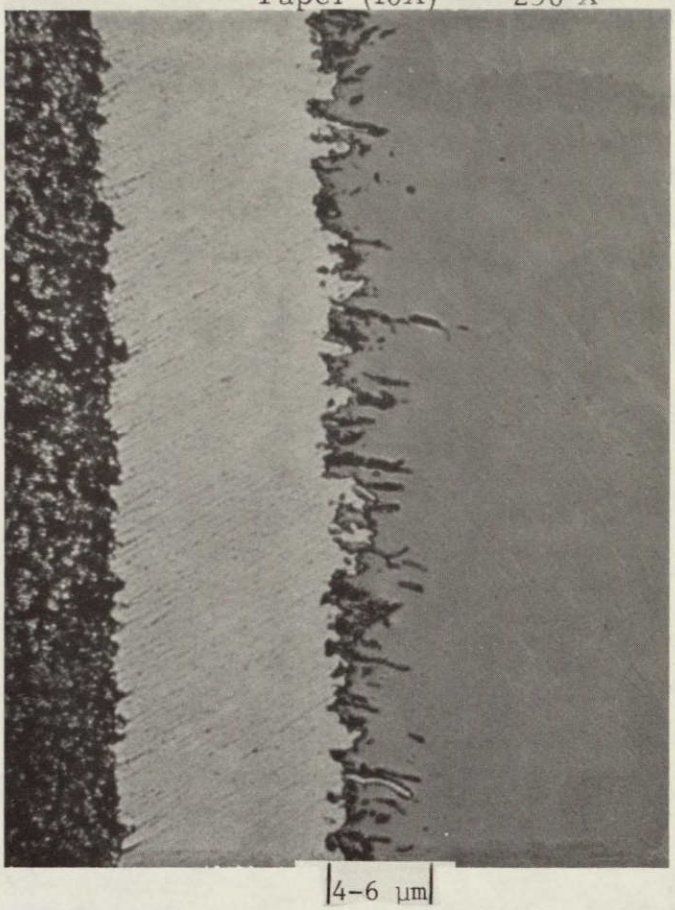

(b)

(c)

Figure 16. The as-polished (a) and etched surfaces (b and c) of a tapered section of (100) as-sliced wafer

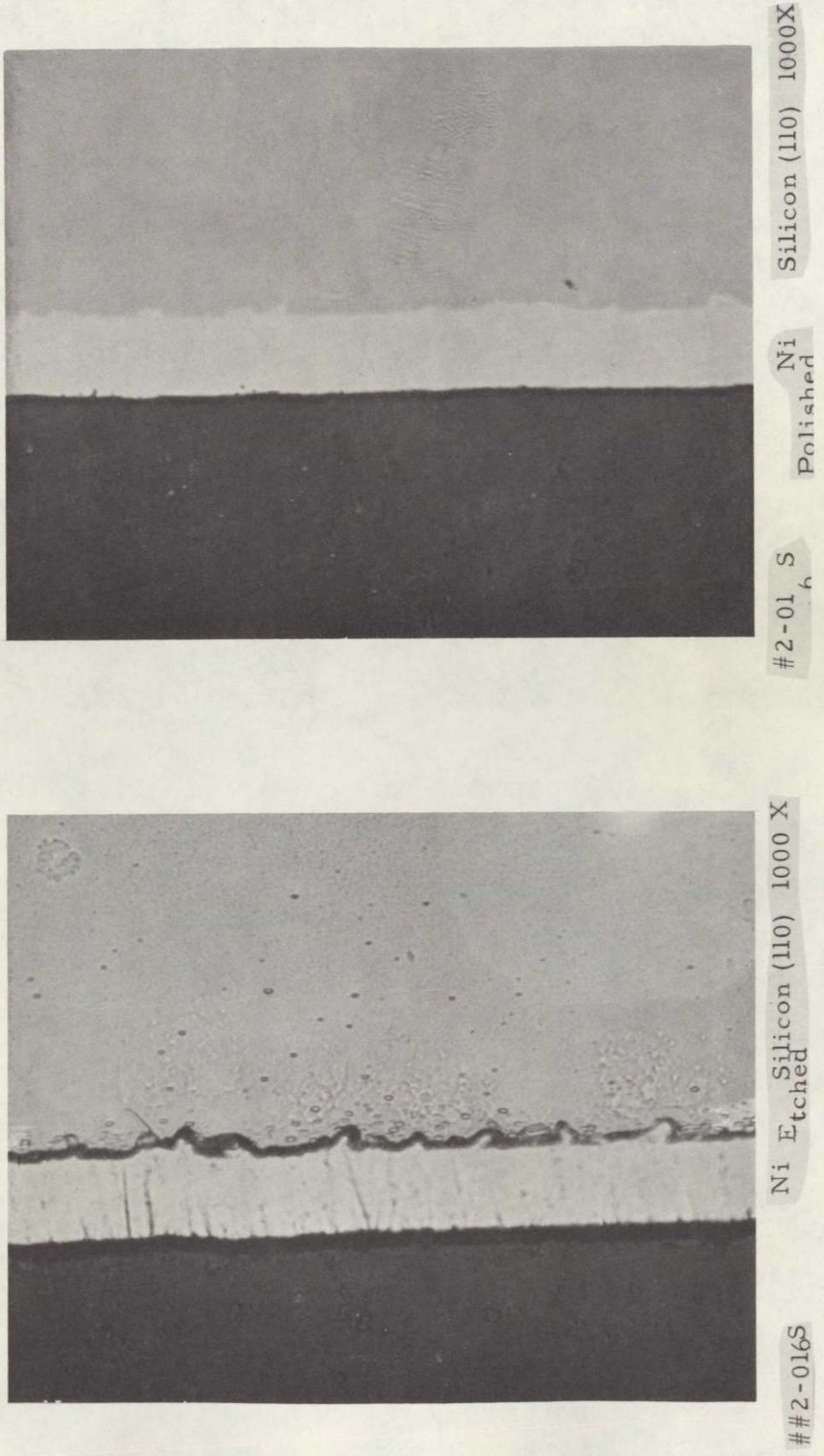

Figure 17. The as-polished and etched cross-section of a sliced wafer. The (110) surface is being viewed (1000X).

ECONOMIC ANALYSIS

The present emphasis of the program is to cast a boule 10 x 10 x 10 cm^3 by the Heat Exchanger Method (HEM). To meet the short term goals (1982) it is intended to cast 20 x 20 x 20 cm^3 size. This boule will be sectioned into four bars 20 x 10 x 10 cm^3 size by a band saw. The bars will then be sliced into wafers by the FAM technique. To meet the long-term goals the ingot size cast will be 30 x 30 x 30 cm^3 which will be sectioned into nine bars of 30 x 10 x 10 cm^3.

The economic analysis has, therefore, been carried out for HEM crystal casting, sectioning into bars and FAM slicing of bars into wafers. This analysis has been carried out based on a plant to produce the firm market demand, viz., 6.7 x 10^4 square meter wafers in 1982 and 1.33 x 10^6 square meter wafers in 1986. SAMICS approach has been adopted using the IPEG equation:

$$\text{Price} = \{(0.49 \times \text{EQPT}) + (97 \times \text{SQFT}) + (2.1 \times \text{SLAB}) + (1.3 \times \text{MATS}) + (1.3 \times \text{UTIL})\} \Big/ \text{QUANTITY}$$

where EQPT = total equipment costs

SQFT = working area in square feet

SLAB = direct labor costs

MATS = direct materials costs

UTIL = utilities costs

In the short-term goals analysis, the growth rate, expendables in HEM casting, slicing rate and labor requirements for FAM slicing have been treated as variables and the effect studied on costs.

SHORT TERM GOALS

Process - HEM crystal casting and FAM slicing
Production - 67,000 square meter silicon wafers
Yield - 95%

Assumptions:

	HEM	SECTION	FAM
Equipment cost, $	45,000	35,000	40,000
Floor space, sq.ft.	60	80	80
Labor, units/operator	10	1	10
Expendables/run, $	95	3	10
Boule size	20 x 20 x 20 cm^3	4(20 x 10 x 10 cm^3) sections	25 wafers/cm

Total Process

HEM Casting
Sectioning: $3.33/m^2
FAM Slicing

Value added costs, $/m^2

HEM Casting → / FAM Slicing ↓	Growth Rate, kg/hr			
	1.0	1.5	2.0	2.5
0.05	34.89	33.23	32.99	32.40
0.10	27.55	25.89	25.65	25.06
0.15	25.49	23.83	23.59	23.00
0.20	23.91	22.25	22.01	21.42
0.25	22.76	21.10	20.86	20.27

Wafer price (based on $25/kg polysilicon), $/m^2

HEM Casting → / FAM Slicing ↓	Growth Rate, kg/hr			
	1.0	1.5	2.0	2.5
0.05	64.98	63.32	63.08	62.49
0.10	57.64	55.98	55.74	55.15
0.15	55.58	53.92	53.68	53.09
0.20	54.00	52.34	52.10	51.51
0.25	52.85	51.19	50.95	50.36

HEM Casting

Value added costs, $\$/m^2$

Growth rate kg/hr	Expendables/run	
	$95	$190
1.0	14.99	21.78
1.5	13.33	20.11
2.0	13.09	20.18
2.5	12.50	19.54

FAM Slicing

Value added costs, $\$/m^2$

Slicing Rate mm/min	Labor, units/operator	
	10	5
0.05	16.57	19.99
0.10	9.23	10.99
0.15	7.17	8.34
0.20	5.59	6.53
0.25	4.44	5.14

LONG TERM GOALS

Process - HEM Crystal Casting and FAM Slicing

Production - 1,330,000 square meter silicon wafers (Firm market in 1986)

Yield - 95%

Assumptions:

	HEM	Sectioning	FAM
Equipment cost, $	30,000	25,000	25,000
Floor space, sq.ft.	60	80	80
Labor, units/ operator	10	1	10
Expendables/ run, $	95	2	5
Cycle time, hrs.	48	8	17
Boule size	30cm x 30cm x 30cm		
Growth rate	2.4 kg/hr		
		9 ($30 \times 10 \times 10 cm^3$) sections	
Slicing rate			25 wafers/cm 0.1 mm/min

Value added price, $\$/m^2$

	HEM	Section	FAM	Total
EQPT	1.77	0.18	1.32	3.26
SQFT	1.12	0.12	0.52	1.78
SLAB	1.14	1.19	0.76	3.08
MATS + UTIL	0.43	0.04	2.04	2.50
	4.46	1.53	4.63	10.62

Polysilicon $\$/kg$	Wafer price $\$/m^2$
10	22.64
17	31.06
25	40.67
50	70.73

CONCLUSIONS

1. HEM cast silicon has shown a solar cell conversion efficiency of 14% (AM1). In spite of the impurities incorporated from the furnace, the efficiency of this material was higher than the control cell.

2. The high V_{oc} and CFF obtained in the HEM cells suggests that it is closer to float-zone silicon quality. This is not surprising as the directional solidification will purify the silicon and reject the impurities in the last material to solidify.

3. Semiconductor grade silica crucibles fabricated with a graded structure have eliminated all ingot cracking problems.

4. Ingots cast in the semiconductor grade graded crucibles only have non-single crystallinity in the bottom corner where the crucible sagged.

5. Heat treatment after solidification has improved the delamination of the square crucibles. The use of faster vitrifying silica crucibles results in distortion of the shape of the square crucibles.

6. A very high degree of crystallinity has been achieved in the square ingots cast.

7. Natural diamonds of 30 μm and 22 μm size can be used for

efficient slicing. However, the cutting performance of explosively formed synthetic diamonds is poorer.

8. Wires electro and electroless plated with 0.3 mil nickel that were not hardened did not perform as well as wires with hardened platings.

9. Heat treatment of electroless nickel plating at 600°F caused embrittlement; therefore, it did not prevent diamond pull out.

10. SEM photographs show wear on the cutting surface of wires with unhardened nickel platings indicating diamond pull-out occurred.

11. The surface damage of wafers sliced with 22 μm diamonds is 4 - 6 μm.

12. Using the Heat Exchanger Method (HEM) of crystal casting and Fixed Abrasive Method (FAM) of multiwire slicing the projected add-on costs for 1982 are $20.27-$34.89 per square meter of silicon wafer. These costs reduce to $10.62 for 1986.

REFERENCES

1. F. Schmid and C. P. Khattak, "Heat Exchanger Method--Ingot Casting/Fixed Abrasive Method--Multi-Wire Slicing (II)," DOE/JPL 954373, Crystal Systems, Inc., Quarterly Progress Report No. 2, April 7, 1978.

2. F. Schmid and C. P. Khattak, "Heat Exchanger--Ingot Casting/Slicing Process," ERDA/JPL 954373, Crystal Systems, Inc., Quarterly Technical Progress Report No. 8, October 1, 1977.

MILESTONES

ITEM	DESCRIPTION
1	2.5 kg HEM crack-free ingot/square cross-section greater than 10 cm x 10 cm
2	Design/fabricate wafering machine
3	Ingot samples/wafer samples
4	Characterization
5	Crucible development
6	Crucible cost studies
7	Growth rate studies
8	Blade development
9	Fabricate/evaluate solar cells
10	Design analysis study
11	Monthly report
12	Quarterly report
13	Annual report

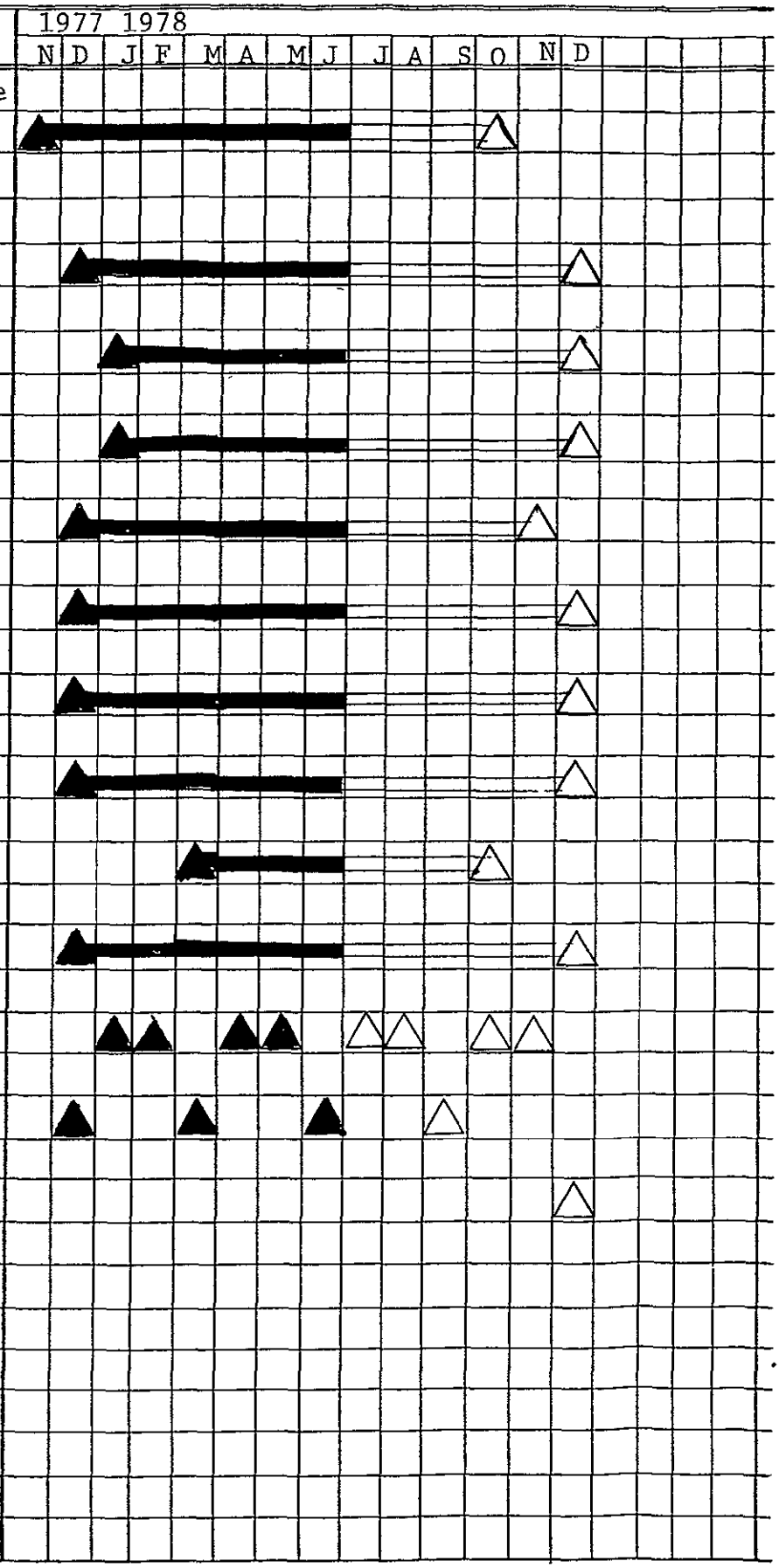

CERAMIC BULLETIN VOL. 57, No. 6 (1978)

Casting Large Silicon Crystals in Clear Silica Crucibles

CHANDRA P. KHATTAK* and FREDERICK SCHMID*

Crystal Systems, Inc., Salem, Mass.

Silicon crystals are being cast by a directional solidification technique[1] which uses a high temperature heat exchanger to extract heat from the bottom of the crystal. This heat-exchanger method (HEM) has been used effectively to grow sapphire crystals (up to 25 cm in diameter and weighing 30 kg) to a high degree of perfection.[2]

A seed crystal is centered at the bottom of a silica crucible, loaded with polycrystalline silicon and seated on the heat exchanger. After being evacuated to 0.1 torr, the crucible is heated in the graphite resistance furnace. The seed is prevented from melting by forcing gaseous helium through the heat exchanger. The distinguishing feature of the HEM is the ability to control independently the solidification interface without moving the crucible, heat zone, or crystal. Since the crystal grows from the bottom to the top, convection currents are suppressed. The solid-liquid interface is surrounded by the melt, thereby preventing the incorporation of impurities which are lighter than silicon (such as SiO and SiO_2) and float to the surface of the melt. These factors minimize the temperature and concentration fluctuations at the growth interface, thus influencing the chemical homogeneity and crystal perfection.[3] A major potential of this process lies in the fact that even inclusions at the solid-liquid interface do not cause any growth instabilities to occur.[4]

Silicon undergoes an expansion during freezing.[5] In a conventional casting process, the outside surfaces will be the first to solidify and the expansion resulting from the freezing of the interior material will then crack the ingot. In the HEM process, the solidification proceeds from the bottom upwards, hence cracking caused by expansion of entrapped liquid is prevented.

The thermal conductivity of silicon in the molten state is more than twice that in the solid state.[6] Thus the extraction of heat by the heat exchanger progressively impedes the rate of growth as the interface proceeds. The problem is further compounded by the decrease in the thermal conductivity of the crucible with the decrease in temperature.[7]

One of the major problems associated with casting silicon in clear, fused-silica crucibles is cracking of the ingot. During solidification, silicon bonds to fused silica and, because of mismatch in the thermal expansion coefficients,[8,9] both the ingot and the crucible fracture during cooling. Ingots viewed with a fiber-optic light source during the cooldown cycle showed that cracking occurred at 650°C. This coincides with the ductile-brittle transformation of silicon.[10] In Fig. 1, microcracking occurs all along the silicon-silica interface. A portion of this interface is magnified in Fig. 2 to illustrate the strong bonding between the ingot and the crucible.

Beryllium or aluminum additions to silicon have prevented cracking of the ingot.[11] However, in the present development of silicon for photovoltaic solar cells, these additions are not desirable. Another solution is the use of a crucible which is strong enough to contain the silicon in the molten stage but cracks itself during the cooldown cycle before enough stresses are built up in the ingot. Hino and Stauss[12] used clear silica crucibles (0.25- to 0.50-mm wall thickness) to produce sound ingots 30 mm in diameter weighing 50 to 100 g. In the present study (to grow crystals 15 cm in diameter and weighing 2–2.5 kg), cracking of the ingot was always observed in fused silica crucibles with a wall 2.5 mm thick. However, when crucibles with walls <1 mm thick were used, the tendency to crack was limited to the immediate vicinity of the silicon-silica interface. Figure 3 shows a cross section of a 2.3–kg ingot cast in a 15-cm-diameter, 1-mm-thick clear, fused-silica crucible. Most of the mate-

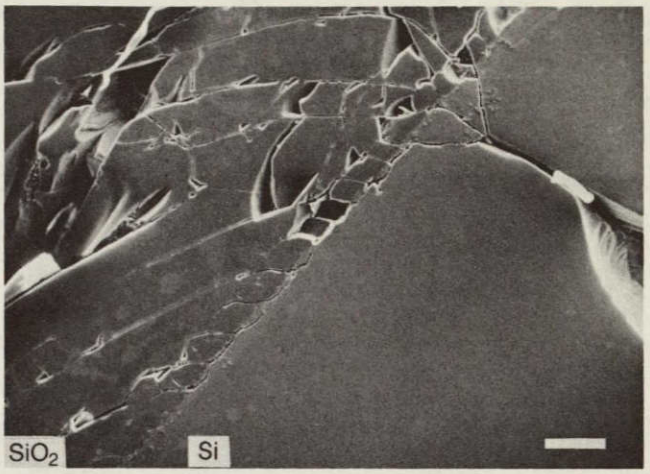

Fig. 1. SEM of SiO_2/Si interface showing cracking problems (20 kV, bar= 100 μm.

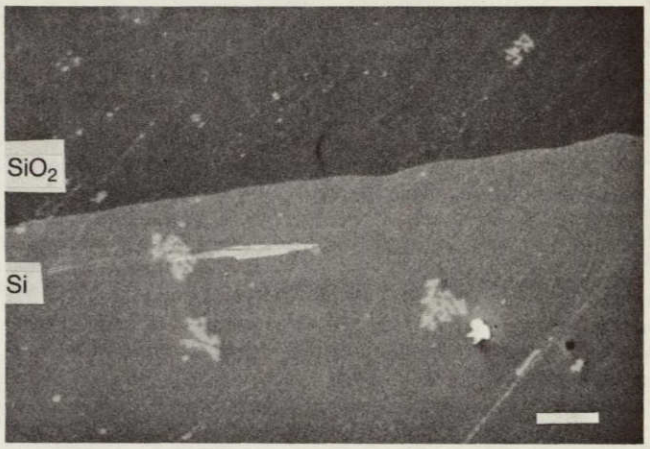

Fig. 2. Section of SiO_2/Si interface showing strong bonding (10 kV, bar= 10 μm).

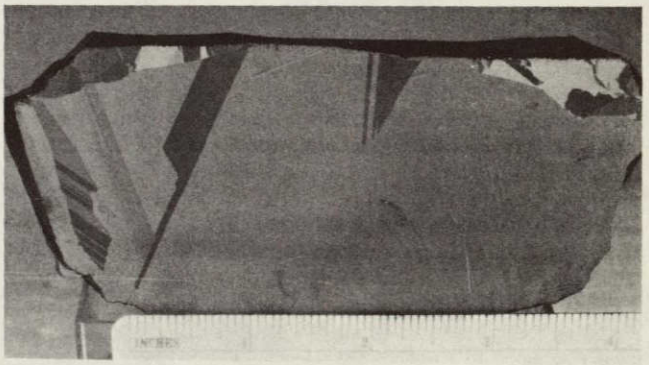

Fig. 3. Polished and etched cross section of "crack-free" Si ingot cast by heat exchanger method.

*Member, the American Ceramic Society.

Sponsored under an interagency agreement between ERDA and NASA.
Received November 4, 1977.

rial is single crystal with some areas where large grains are observed. Such structure should be acceptable for processing into solar cells for terrestial applications.[13] Other properties such as a dislocation density of 100/cm² and minority carrier diffusion length of 31 μm were reported earlier[4] for material grown by this method.

In conclusion, it has been demonstrated that silicon forms a tenacious bond with clear fused silica, which results in cracking of the ingot during the cooldown cycle. This cracking tendency can be limited to the outside surface of the ingot by using thin-wall crucibles. The heat-exchanger method has produced silicon ingots 15 cm in diameter and weighing 2.3 kg for use as material for solar cells in terrestial applications.

References

[1] F. Schmid and D. Viechnicki, "Growth of Sapphire Disks from the Melt by a Gradient Furnace Technique," *J. Am. Ceram. Soc.*, **53** [9] 528–29 (1970).

[2] D. Viechnicki and F. Schmid, "Crystal Growth Using the Heat Exchanger Method (HEM)," *J. Cryst. Growth*, **26** [1] 162–64 (1974).

[3] K. M. Kim, A. F. Witt and H. C. Gatos, "Crystal Growth from the Melt and Destabilizing Thermal Gradients," *J. Electrochem. Soc.*, **119** [9] 1218–26 (1972).

[4] T. Digges, Jr., M. H. Leipold, K. M. Koliwad, G. Turner and G. D. Cumming, "Some Observations on the Characteristics of Low-Cost Silicon Sheets"; presented at the IEEE Photovoltaic Specialists Conference, Baton Rouge, La., 1976.

[5] E. Billig, "Some Defects in Crystals Grown from the Melt: 1. Defects Caused by Thermal Stresses," *Proc. Roy. Soc.*, **A235**, 37–55 (1956).

[6] Yu. M. Shashkov and V. P. Grishin, "Thermal Conductivity of Silicon in the Solid and Liquid States near the Melting Point," *Sov. Phys. Solid State*, **8** [2] 447 (1966).

[7] R. W. Powell, C. Y. Ho and P. E. Liley, "Thermal Conductivity of Selected Materials," *Natl. Bur. Stand.*, **NBS-8**, Category 5, 99–106 (1966).

[8] D. F. Gibbons, "Thermal Expansion of Some Crystals with the Diamond Structure," *Phys. Rev.*, **103**, 569–71 (1956).

[9] P. H. Gaskell, "Thermal Properties of Silica: 2," *Trans. Faraday Soc.*, **62** [6] 1505–1510 (1966).

[10] G. L. Pearson, W. T. Read Jr. and W. L. Feldman, "Deformation and Fracture of Small Silicon Crystals," *Acta Metall.*, **5** [4] 181–91 (1957).

[11] H. C. Torrey and C. A. Witmer, Crystal Rectifiers. McGraw-Hill Book Co., New York, N.Y., 1948.

[12] J. Hino and H. E. Stauss, "Melting of Undoped Silicon Ingots," *J. Metals*, **4** [6] 656 (1952).

[13] R. K. Mueller and R. L. Jacobson, "Grain Boundary Photovoltaic Cell," *J. Appl. Phys.*, **30** [1] 121–22 (1959). □